THE JOURNAL OF PHYSICAL CHEMISTRY C

Article

pubs.acs.org/JPCC

How the Second-Order Nonlinear Optical Response of the Collagen Triple Helix Appears: A Theoretical Investigation

Marc de Wergifosse,[†] Jérôme de Ruyck,[‡] and Benoît Champagne*[,†]

[†]Laboratoire de Chimie Théorique and [‡]Laboratoire de Chimie Biologique Structurale, Unité de Chimie Physique Théorique et Structurale, Université de Namur, rue de Bruxelles, 61, B-5000 Namur, Belgium

Supporting Information

ABSTRACT: The origin and the nature of the first hyperpolarizability of collagen has been unraveled by performing first-principles calculations on the PPG10 compound, a molecular model for the collagen triple helix structure, and on its building blocks. The first hyperpolarizability of the triple helix originates from the amide groups. Owing to the rigidity of the structure and of the proline units, the β-tensor components parallel to the helical axis add to each other, whereas the perpendicular components cancel each other, which result in a dipolar first hyperpolarizability and a depolarization ratio close to 9. The calculations have also shown that the resulting β values cannot be viewed as the simple sum of the amide group contributions. Indeed, for a given chain, the β per amino acid increases with the size of the chain, whereas the β of the triple helix is smaller than three times the β of a single chain. The calculations, performed at different levels of approximation, demonstrated also the reliability of the ONIOM scheme when combining high and low layers described with different basis sets and the weak impact of electron correlation.

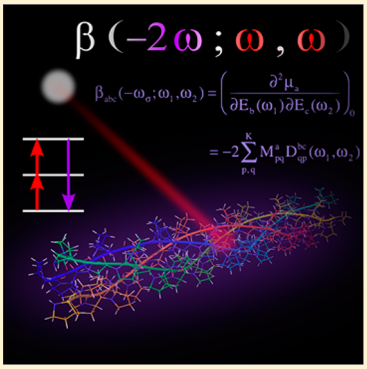

I. INTRODUCTION

Second-harmonic imaging microscopy (SHIM) is a high-resolution biomedical imaging technique, which has been developed to get contrast enhancement of noncentrosymmetric molecular arrangements.[1−9] In their review, Campagnola and Loew[1] report that the first biological second-harmonic generation (SHG) imaging experiment was done in 1986 by Freund et al.[10] on collagen of rat-tail tendon. It revealed the existence of a discrete network of fine, polar, filamentous, or columnar structures and also the presence of strongly polar surface or near-surface patches. It is now known that biological materials can be highly polarized and often assemble into large, ordered noncentrosymmetric structures. Because noncentrosymmetry is essential to achieve SHG signal, information about the molecular organization of chromophores and structural proteins can be extracted from SHIM. Indeed, many of different endogenous tissues present SHG signals. The determination of the molecular origin of this response is difficult to elucidate, but collagen has been clearly identified as one of the principal SHG causes.[10,11] Collagen is one of the most present proteins in the animal kingdom, and many genetically distinct collagen types exist.[12,13] Collagen is a three polypeptide α chain, where the Gly-X-Y monomer is the repeated unit. Proline and 4-hydroxyproline frequently occupy the X and Y positions, respectively. The glycine units give the flexibility to the chains to make three left-handed helices, which are held together by interchain hydrogen bonds.

Measurement of the second-order hyperpolarizability of the collagen triple helix by hyper-Rayleigh scattering (HRS) experiment has been done by Deniset-Besseau et al.,[14] who characterized the first hyperpolarizability (β) of collagen from rat-tail tendon as well as a short model of triple-helical peptides $[(\text{Pro-Pro-Gly})_{10}]_3$ (PPG10). They concluded that the collagen large second-order nonlinear optical (NLO) response originates from the tight alignment of a large number of small and weakly efficient harmonophores, presumably the peptide bonds and not from a particular amino acid, resulting in an amplification of the nonlinear signal. Following this study, in 2010, Loison and Simon[15] applied an additive model to theoretically determine β of PPG10, while they wrote that, "For large polymers such as proteins, precise quantum chemical calculations of the hyperpolarizability are beyond the reach of today's computer power." In their study, they showed that the additive model using *N*-methylacetamide as a building block leads to β results that agree qualitatively with HRS data from ref 14. In 2011, Tuer et al.[16] approximated the β tensor of the collagen triple-helix models by taking the sum of the β tensors of the constitutive amino acids with the time-dependent Hartree−Fock method and accounting for the peptide bond contributions. They applied the unit sphere representation for a 3-D visualization of the β tensor.[17] Recently, Alparone[18] investigated α-helix and β-strand of oligoglycines with ab initio methods and showed that for the longest chains, the response of the β-strand is one order of magnitude larger than for the α-helix. Moreover, Wei et al.[19] used the summation-over-states (SOS) method combined with configuration interaction singles

Received: February 14, 2014
Revised: March 25, 2014
Published: March 25, 2014

   dx.doi.org/10.1021/jp501602a | *J. Phys. Chem. C* 2014, 118, 8595−8602

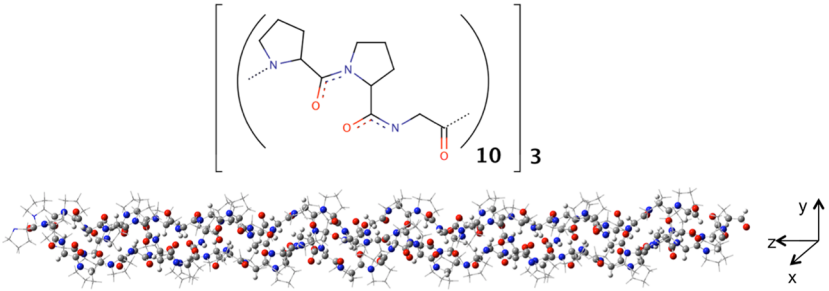

Figure 1. Sketches of PPG10 as well as its optimized geometry, where the ONIOM high layer is represented with balls and sticks and the low layer is represented with sticks.

calculations to highlight the impact of a single amino acid mutation in α-helical polyalanine. They showed that side chains containing benzene, phenol, and indole have large contributions to the polarizability and first hyperpolarizability. However, analyzing the amplitudes and variations of the polarizability raises doubt on the convergence of their SOS expressions, which include only 50 excited states for a system containing 17 amino acids. After having modeled the β of several fluorescent proteins with the ONIOM (our own n-layered integrated molecular orbital and molecular mechanics) method where the surroundings of the chromophore as well as the electron correlation effects are accounted for,[20] here we study the first hyperpolarizability of PPG10 with quantum chemical methods. The purpose of this study is (i) to further unravel the structure−property relationships associated with the β response and (ii) to validate a first-principles method able to accurately describe this large system. This is carried out by using the ONIOM method,[21] which consists of partitioning the system in several layers described at different levels of theory, where the peptide backbone is treated with the high-level method of calculation and the chain ends as well as the remainders of proline rings with the low level of calculation.

II. MATERIALS AND METHODS

II.A. Theoretical and Computational Aspects. The structure was taken from X-ray diffraction data to investigate the collagen-like triple-helix polypeptide $[(\text{Pro-Pro-Gly})_{10}]_3$.[22] After the addition of the hydrogen atoms, the PPG10 geometry (Figure 1) was optimized with the semiempirical PM6 method. Note that the geometry optimization procedure leads to a negligible chain rebuilding, as evidenced by the variation of the distance between the chain extremities (taken as terminal N and C atoms) from 82.2 to 82.6 Å. To compare different levels of theory, a $[(\text{Pro-Pro-Gly})_3]_3$ (PPG3) fragment was cut from the large PPG10. Its geometry was optimized using the ONIOM B3LYP/6-311G**:PM6 method, where the chain of peptide bonds was treated with the high level of calculation and the remainder with the low level of calculation (Figure 2). Then, the PPG3 structure was modified to build the $[(\text{Gly-Gly-Gly})_3]_3$ (GGG3) structure, which was optimized at the B3LYP/6-311G** level of calculation, as well as the Pro-Pro-Gly monomer.

To characterize β of PPG10, which for today's computers is a very large system (1035 atoms), we used the ONIOM scheme in combination with the time-dependent Hartree−Fock (TDHF) method to obtain the dynamic β and with the coupled-perturbed Hartree−Fock (CPHF) method for the static one. In the two-layer ONIOM approximation, the system is partitioned in high (the peptide backbone) and low (the lateral groups) layers (Figures 1 and 2), which are investigated by a high/low-level of theory, respectively. The corresponding ONIOM first hyperpolarizability tensor reads

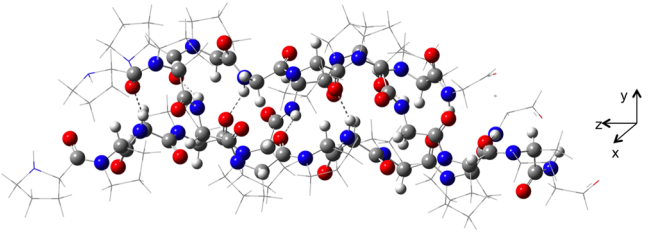

Figure 2. Optimized geometry of $[(\text{Pro-Pro-Gly})_3]_3$ where the ONIOM high layer is represented with balls and sticks and the low layer is represented with sticks.

$$\vec{\vec{\beta}}_{\text{ONIOM}} = \vec{\vec{\beta}}_{\text{real,low}} - \vec{\vec{\beta}}_{\text{model,low}} + \vec{\vec{\beta}}_{\text{model,high}}$$

because the ONIOM scheme allows for a consistent treatment of the molecular properties related to the responses to static and dynamic electric fields.[21] $\vec{\vec{\beta}}_{\text{real,low}}$ is the first hyperpolarizability tensor of the entire or real system evaluated at the low level of approximation, whereas $\vec{\vec{\beta}}_{\text{model,low}}$ and $\vec{\vec{\beta}}_{\text{model,high}}$ are the corresponding tensors for the model system (here the peptide backbone) calculated at the high and low levels of approximation, respectively. This expression follows the energy expression given in ref 21. For each subcalculation, the static and dynamic tensors are determined using the TDHF or CPHF schemes, respectively. We employed the polarizable continuum model within the integral equation formalism (IEFPCM) to take into account the solvent (water) effects.[23,24] In the ONIOM method, for each subcalculation, the cavity of the real system was used.[25]

Considering previous investigations,[18,26] the HF/6-31+G* method is initially chosen as the high level of theory for calculating the β tensors, while in a second step electron correlation effects were assessed to provide more quantitative estimates. The 6-31+G* basis set is a good compromise between accuracy and computational resources, whereas the HF method is known to underestimate the first hyperpolarizability of push−pull π-conjugated systems owing to missing electron correlation effects, but generally it turns out to be suitable to provide trends among compounds. Moreover, a long-range corrected (LC) exchange-correlation functional, LC-BLYP[27,28] (with a range-separating parameter μ of 0.47), in combination with the time-dependent density functional theory (TDDFT) scheme was also employed to provide an estimate of

dx.doi.org/10.1021/jp501602a | J. Phys. Chem. C 2014, 118, 8595−8602

the impact of electron correlation, while describing exactly the long-range behavior of exchange. Indeed, this method is reliable for describing the changes of β upon enlarging the π-conjugated linker of push−pull π-conjugated systems, although it also underestimates systematically the CCSD(T) (coupled cluster method including the single and double and a perturbative estimate of the triple excitations) reference values.[26] As it was impossible to perform full TDHF/CPHF calculations with 6-31+G(d) basis set on PPG10, the validation of the ONIOM method was done on the small PPG3 system by comparing it to TDHF and TDDFT reference calculations. For the low level of theory, the HF/6-31G(d) method was selected. To further investigate electron correlation effects on the first hyperpolarizabilities of the PPG monomer, additional Møller−Plesset second-order perturbation theory (MP2) calculations were performed within the finite field (FF) procedure.[29] To remove higher order contaminations in the finite differentiation procedure and achieve good accuracy (1−10 au) on the numerical derivatives, the Romberg method was applied. The field-dependent energies were calculated for field amplitudes of 0.0004×2^n with $n = 0-4$. To account for frequency dispersion at the MP2 level, we employed the multiplicative approximation.[30]

Experimentally, the first hyperpolarizabilities and their depolarization ratios (DRs) were determined from HRS measurements.[31] These are related to the intensity of the vertically polarized (along the Z axis) signal scattered at 90° with respect to the propagation direction (Y axis) for a nonpolarized incident light beam. β_{HRS} and DR read

$$\beta_{HRS}(-2\omega;\, \omega,\, \omega) = \sqrt{\{\langle\beta_{ZZZ}^2\rangle + \langle\beta_{ZXX}^2\rangle\}}$$

$$DR = \frac{I_{VV}^{2\omega}}{I_{HV}^{2\omega}} = \frac{\langle\beta_{ZZZ}^2\rangle}{\langle\beta_{ZXX}^2\rangle}$$

where $\langle\beta_{ZZZ}^2\rangle$ and $\langle\beta_{ZXX}^2\rangle$ are orientational averages of the $\vec{\vec{\beta}}$ tensor, which are proportional to the scattered signal for vertically and horizontally polarized incident light beams, respectively. DR reveals the shape of the NLO-phore. Full expressions for these brackets without assuming Kleinman's conditions can be found in ref 32. The analysis of the β tensor also adopts the unit sphere representation,[16,17] which defines an effective SHG dipole vector according to

$$\vec{\beta}_{eff} = \vec{\vec{\beta}} : \vec{E}(\theta,\, \phi)\vec{E}(\theta,\, \phi)$$

$\vec{E}(\theta,\phi)$ is a unit vector of incident electric field, of which the polarization is defined in spherical coordinates (θ,ϕ). On the unit sphere surface around the molecule, $\vec{\beta}_{eff}$ is drawn at each point (θ,ϕ), representing the polarization and the magnitude of the generated second-harmonic response for that particular incident field $\vec{E}(\theta,\phi)$.

All reported β values are given in au [1 au of $\beta = 3.6213 \times 10^{-42}$ m^4 V^{-1} = 3.2064×10^{-53} C^3 m^3 J^{-2} = 8.639×10^{-33} esu] within the T convention. All calculations were done with the Gaussian09 package,[33] except for the geometry optimization of PPG10, which was carried out with the MOPAC package.[34]

II.B. Materials and Experimental Spectroscopic Characterizations. In ref 14, the first hyperpolarizability of PPG10 was experimentally determined by frequency-resolved femtosecond HRS. To estimate the intrinsic β response, these experimental data were pretreated by ourselves to eliminate the resonance effects.[35,36] The frequency dispersion factors, $F(\omega,\omega_{ge},\gamma) = \beta_{zzz}(-2\omega;\omega,\omega)/\beta_{zzz}(0;0,0)$, were determined from successive refinements of the two-state approximation (TSA).[37] $\hbar\omega_{ge}$ is the excitation energy of the dominant excited state, and γ is the damping factor. Besides the conventional TSA, (i) homogeneous damping was taken into account, (ii) then, an inhomogeneous broadening based on the absorption spectrum, which implicitly contains information on the distribution of the transition frequencies, and (iii) finally, the later scheme was extended to account for the vibronic structure of the excited states.[35,36] (See more details in SI.) The successive $F(\omega,\omega_{ge},\gamma)$ functions had to be fitted to the UV absorption spectrum to apply these extrapolation schemes. As a matter of fact, UV/vis absorption spectra were recorded.

The absorption spectrum of PPG10 was obtained using an Uvikon$_{XS}$ spectrophotometer from BIO-TEK instruments. Samples were prepared by mixing $(Pro\text{-}Pro\text{-}Gly)_{10}$ (Peptides International, OPG-4006) solutions with acetic acid 0.5 mM to obtain a final $(Pro\text{-}Pro\text{-}Gly)_{10}$ concentration of 0.6 mg·mL^{-1}, which self-organizes to form triple helices. The solutions were then gently stirred for 24 h at 4 °C. A spectrum of the buffer only was recorded as a blank. The difference between the PPG10 and blank solutions gives the experimental spectrum (Figure 3). The $F(\omega,\omega_{ge},\gamma)$ function was then fitted to get the parameters listed in Table 1.

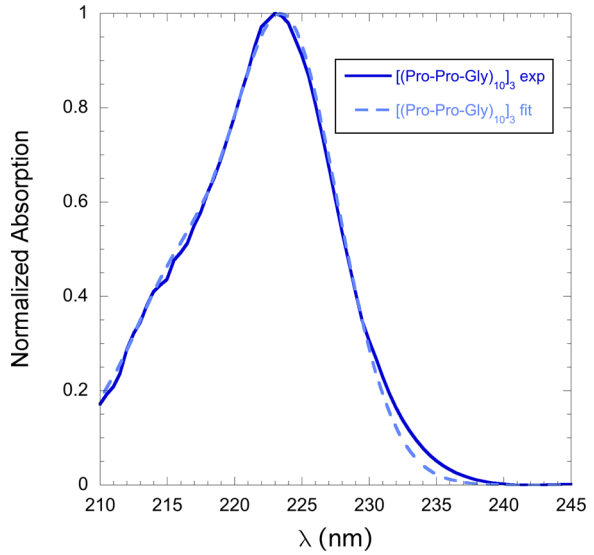

Figure 3. Normalized absorption spectrum of PPG10. The full line corresponds to the experimental data, while the dashed line corresponds to the fitted spectrum.

Dynamic light scattering (DLS) experiments were performed using a DynaPro NanoStar DLS/SLS recorder from Wyatt Technology Corporation. These results demonstrate that there

Table 1. Parameters Fitting the UV/vis Absorption Spectrum[a]

$\hbar\omega_{ge}$ (eV); λ_{eg} (nm)	5.54; 224
$\gamma_{homogeneous}$ (eV)	0.181
$\gamma_{inhomogeneous}$ (cm^{-1})	100
S, Huang−Rhys factor	0.40
ω_{vib} (cm^{-1})	1700
γ_{vib} (cm^{-1})	1100

[a]See the SI for more details on the parameters.

dx.doi.org/10.1021/jp501602a | J. Phys. Chem. C 2014, 118, 8595−8602

Table 2. β_{HRS} of $[(Pro\text{-}Pro\text{-}Gly)_3]_3$ and $[(Gly\text{-}Gly\text{-}Gly)_3]_3$ Calculated at Different Levels of Approximation (in au)

	TDHF/CPHF 6-31+G(d)				TDDFT/LC-BLYP 6-31+G(d)			
	PPG3		GGG3		PPG3		GGG3	
	in vacuo	in water (IEFPCM)	in vacuo	in water (IEFPCM)	in vacuo	in water (IEFPCM)	in vacuo	in water (IEFPCM)
$\beta_{HRS,\infty}$	517	1065	474	870	472	1101	461	948
$\beta_{HRS,1900nm}$	539	724	492	661	500	721	484	697
$\beta_{HRS,1064nm}$	591	793	534	718	570	818	541	779

is no oligomerization of the PPG10 triple helices in solution and therefore that the β_{HRS} measurements from ref 14 refer to PPG10 and not some of its aggregates.

III. RESULTS AND DISCUSSION

III.A. Assessment of the ONIOM Method and of Electron Correlation Effects. To reduce the computational costs for calculating the first hyperpolarizability of PPG10, we adopted the ONIOM scheme, where the low and high layers are treated with different basis sets, 6-31G(d) for the low level and 6-31+G(d) for the high one. In addition, the low-level calculations are carried out using the HF method. This approach was first validated by performing calculations on PPG3, for which full 6-31+G(d) calculations could be carried out (Table 2). ONIOM results obtained at the TDHF and TDDFT/LC-BLYP levels are listed in Table 3, demonstrating

Table 3. β_{HRS} of $[(Pro\text{-}Pro\text{-}Gly)_3]_3$ As Calculated with the ONIOM Method (in au)

	ONIOM HF/6-31+G(d): HF/6-31G(d)		ONIOM LC-BLYP/ 6-31+G(d): HF/6-31G(d)	
	in vacuo	in water (IEFPCM)	in vacuo	in water (IEFPCM)
$\beta_{HRS,\infty}$	530	1046	503	1071
$\beta_{HRS,1900nm}$	550	731	527	734
$\beta_{HRS,1064nm}$	599	796	588	816

that the use of a smaller basis set for the lateral groups of the peptide chains has only a minor effect on the β_{HRS} response. Indeed, the CPHF (CPKS/LC-BLYP) static reference values are at most overestimated by 2.5% (6.5%) in vacuo or underestimated by 1.8% (2.8%) when accounting for the solvent, whereas for the dynamic responses, the differences are smaller.

As shown for push−pull π-conjugated systems[26] and small reference molecules for NLO,[38] the electron correlation issue is also briefly addressed here in view of comparison with the experimental data of Deniset-Besseau et al.[14] A first comparison between the HF and LC-BLYP data (Table 2) demonstrates that at most the HF level underestimates the LC-BLYP β_{HRS} values by 8.2% (when accounting for solvent effects), or it overestimates them by at most 9.5% (in vacuo). These effects are very small in comparison with those found for other systems.[26,38] To further substantiate these results, we have performed additional calculations on a unique Pro-Pro-Gly chain, which allows comparisons with the MP2 method (Table 4). The MP2 results are typically 4% larger than the HF one, confirming the small electron correlation effects for β_{HRS} of collagen chains. The HF versus LC-BLYP results are consistent with those of Table 2. These results demonstrate that qualitative and semiquantitative estimates of β_{HRS} of collagen chains can already be obtained at the HF level.

Considering a larger basis set for PPG gives similar results with an increase of less than 8% for aug-cc-pVDZ with respect to 6-31+G(d) and of 6% for aug-cc-pVTZ (Table S1, Supporting Information).

Table 4. β_{HRS} of Pro-Pro-Gly Calculated at Different Levels of Theory with the 6-31+G(d) Basis Set (in au)

in vacuo	TDHF/CPHF	TDDFT LC-BLYP	MP2
$\beta_{HRS,\infty}$	54	48	56
$\beta_{HRS,1900nm}$	55	50	57
$\beta_{HRS,1064nm}$	58	54	60

III.B. Structure−Property Relationships. In the previous paragraph, the choice of high layer to be the chain of peptide bonds was based on the hypothesis that it is responsible for most of the HRS response because the C(=O)−N units are the only π-conjugated parts of PPG10. This is now substantiated by first comparing β_{HRS} of PPG3 to β_{HRS} of GGG3, where only the chains of peptide bonds remain (Table 2). For all dynamic β_{HRS}, the differences between GGG3 and PPG3 are smaller than 10%, whereas they could be slightly larger in the static limit when accounting for the solvent effects. This demonstrates that the β_{HRS} response originates from the peptide backbone. Nevertheless, PPG3 and GGG3 differ by their rigidity. The GGG3 chain is more flexible, which allows the formation of four additional H-bonds, whereas the presence of proline units in PPG3 constrains its conformation.

To further confirm this hypothesis of the peptide backbone origin of β_{HRS}, we have compared the response of one chain of PPG3 with the response of its different building blocks (Table 5). These calculations were performed by keeping the same geometry as in the triple helix. The corresponding unit sphere representations are given in Figure 4. For a single amino acid, the response originates from the asymmetric electron distribution around the heteroatoms, and the effective SHG dipole vector is oriented almost parallel to the C=O bond. These responses are largely dipolar, with DR larger than 6.5 or 7.5. By linking two amino acids, a peptide bond is created, and the amide moiety brings a charge-transfer contribution to the total first hyperpolarizability. Although the compounds are two times larger than the monomer, the β_{HRS} value remains similar or even decreases. Moreover, the shape of the tensor becomes more complex. This is attributed to the amide function contribution combined with those of C=O group, which are differently oriented. This is also evidenced by the smaller DR. Then, going to the tripeptide, the β_{HRS} value increases, which is attributed to the mostly additive contributions of the two amide bonds. By increasing the size of the system, the contribution in the other directions becomes more and more negligible, leading to an overall response along the backbone. This is evidenced by the increase in the DR from the dipeptide to the nonapeptide with a DR of 8.27 for $(Pro\text{-}Pro\text{-}Gly)_3$. In parallel, the nonlinear anisotropy parameter $\rho = |\beta_{J=3}|/|\beta_{J=1}|$, which gives the ratio of

dx.doi.org/10.1021/jp501602a | J. Phys. Chem. C 2014, 118, 8595−8602

Table 5. β_{HRS}, DR (depolarization ratio), and ρ (nonlinear anisotropy factor) for (Pro-Pro-Gly)$_3$ As Well As of Its Different Building Blocks (in au)

	$\beta_{HRS,\infty}$ CPHF 6-31+G(d)	DR	ρ
Pro1	41	7.67	0.35
Pro2	46	6.57	0.53
Gly3	40	7.72	0.35
Pro1-Pro2	40	1.68	4.92
Pro2-Gly3	33	3.73	1.17
Pro1-Pro2-Gly3	58	3.21	1.41
Pro1-Pro2-Gly3-Pro4	95	3.91	1.11
Pro1-Pro2-Gly3-Pro4-Pro5	111	4.21	1.01
Pro1-Pro2-Gly3-Pro4-Pro5-Gly6	127	6.32	0.57
(Pro-Pro-Gly)$_3$	216	8.27	0.25

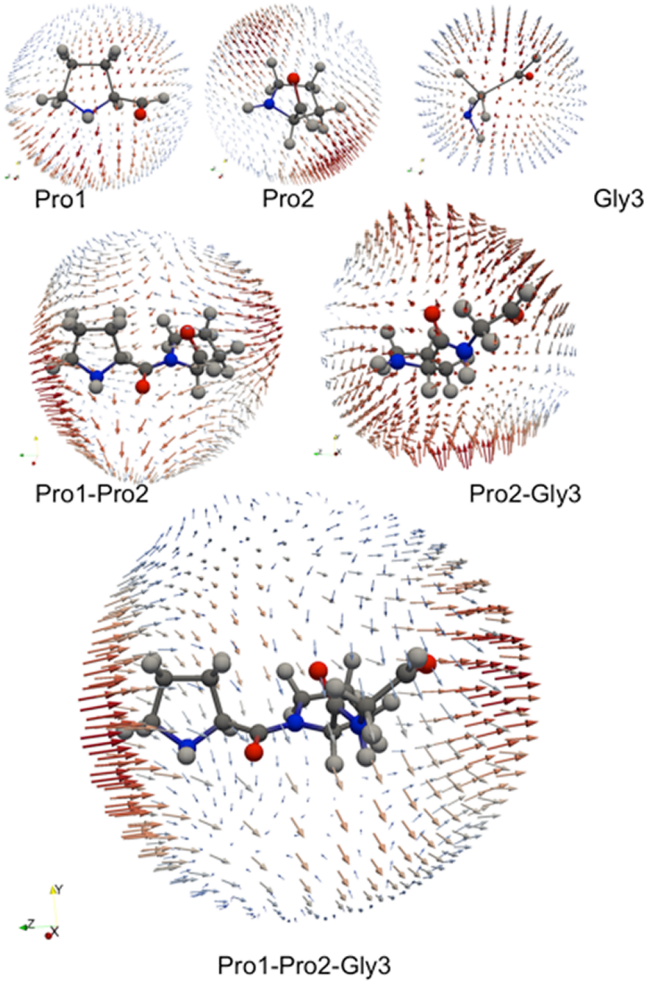

Figure 4. Unit sphere representations of the first hyperpolarizability tensor obtained at the CPHF/6-31G(d) level of calculation for the (Pro-Pro-Gly) chain and its building blocks.

the octopolar versus dipolar contributions to β,[38] decreases, leading to a mostly dipolar response.

Thus, in PPG10, the conformation of the triple helix orients the amide π-conjugated segments around the helical axis so that when the chain grows the radial component vanishes and the axial component becomes dominant. This differs from pyridine−pyrimidine and hydrazine−pyrimidine oligomers, where the radial component is dominant.[39] To some extent, this constrained conformation can be associated with the rigidity of the proline units. To support this hypothesis, we compared the conformations of PPG3 and GGG3 on the basis of the orientation of key bonds with respect to the helical axis (or z-axis). The selected angles are α = ∠OCz, β = ∠NCz, and γ = ∠OCN. Note that if the ∠OCN plane formed by the amide function contains the z axis, γ is equal to $\alpha + \beta$. Data in Tables S2 and S3 in the Supporting Information show that the successive α and β angles of the three chains of PPG3 display the same pattern, demonstrating more regularity and rigidity than in the case of the three chains of GGG3, for which the angle values are more random. This regularity is at the origin of the strong dipolar nature of β in PPG3 and PPG10, and it also explains its larger β_{HRS} value than in GGG3.

Consequently, for PPG10, β_{zzz} is the major β-tensor component. Nevertheless, two other tensor components, $\beta_{xxz} = \beta_{xzx} \approx \beta_{zxx}$ and $\beta_{yyz} = \beta_{yzy} \approx \beta_{zyy}$, are not negligible but more than two or three times smaller than β_{zzz}, respectively. Consistently with this tensor analysis, the DR, which gives information on the shape of the NLOphore, amounts to 8.8 [ONIOM HF/6-31+G(d):HF/6-31G(d), in vacuo]. Moreover, the nonlinear anisotropy parameter ρ is as low as 0.113 for PPG10. Thus, the β response is dominantly dipolar.

To unravel the impact of the triple helix, starting from the geometry of PPG3, the dipole moments and first hyperpolarizabilities have been calculated for PPG2 and PPG1, which are obtained by removing one or two of the PPG chains, respectively. Going from one to two chains, the β_{HRS} response almost doubles, but saturation appears when adding the third chain (Table 6). Similar effects are observed for the $\vec{\beta}$ and $\vec{\mu}$ norms. Figure S2 in the Supporting Information shows how the $\vec{\beta}$ and $\vec{\mu}$ vectors are closely parallel to the helical axis and how small the angle is between them, in particular, for the triple helix. The dipolar behavior of the β response and its orientation are further confirmed in Figure 5, with the unit sphere representation of the β tensor of PPG10, highlighting that the maximum SHG response is obtained for an incident electric field parallel to the triple helix axis. See also Figure S3 in the Supporting Information for the corresponding unit sphere representations for PPG1, PPG2, and PPG3, associated with

Table 6. Static β_{HRS} and Related Quantities for PPG3 and Its Derivatives Obtained after Removing One (PPG2) or Two (PPG1) Chains As Determined at the CPHF/6-31+G(d) Level of Approximation (in vacuo)

	β_{HRS} (au)	DR	$\|\vec{\beta}\|$ (au)	$\|\vec{\mu}\|$ (au)	$\theta_{\vec{\mu},\vec{\beta}}$ (degrees)
PPG3	517	8.47	1403	15.43	7.6
PPG2	410	8.29	1109	13.54	12.6
PPG1	216	8.27	582	7.30	3.7

dx.doi.org/10.1021/jp501602a | J. Phys. Chem. C 2014, 118, 8595−8602

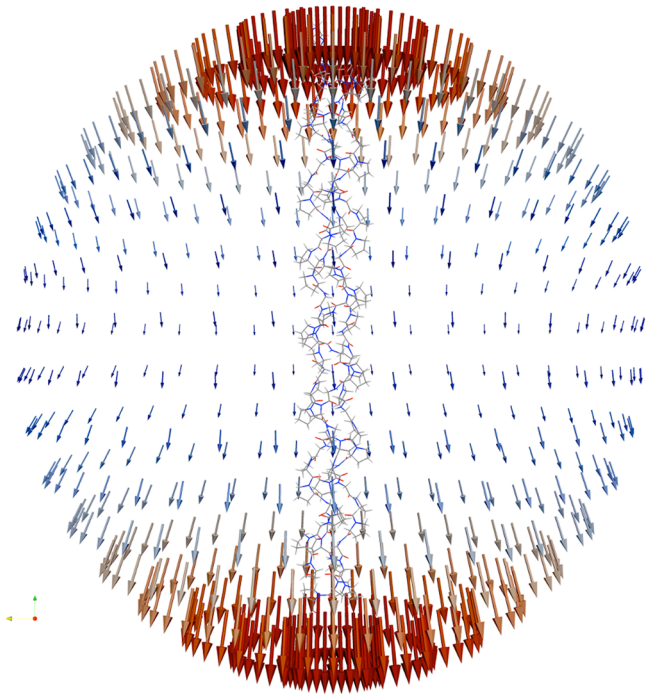

Figure 5. Unit sphere representation of the first hyperpolarizability tensor of PPG10 obtained with the ONIOM HF/6-31+G(d):HF/6-31G(d) method at 1900 nm in water solvent (IEFPCM).

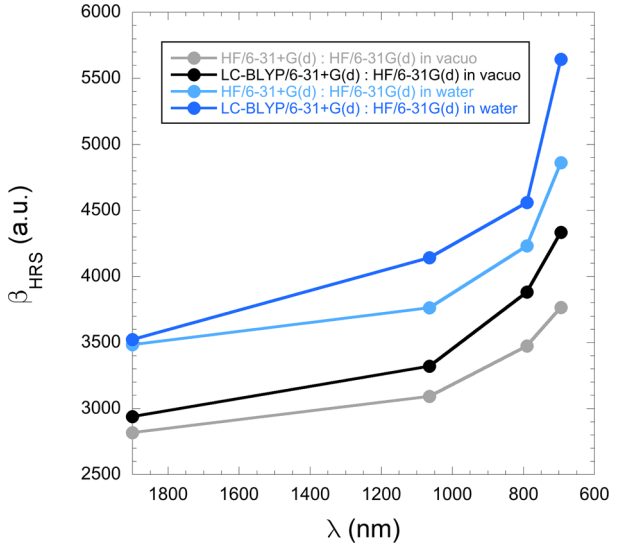

Figure 6. Frequency dispersion of β_{HRS} calculated with the ONIOM HF/6-31+G(d):HF/6-31G(d) and LC-BLYP/6-31+G(d):HF/6-31G(d) methods.

the results in Table 6, where the orientation of the response is similar but the intensity is increasing.

III.C. $[(Pro\text{-}Pro\text{-}Gly)_{10}]_3$: Results and Confrontation to Experiment. The PPG10 β_{HRS} values show an increase by more than a 10/3 factor with respect to PPG3 (Table S4 in the Supporting Information). Considering the effects of the solvent, the β_{HRS}(PPG10)/β_{HRS}(PPG3) ratio, evaluated at the ONIOM level, amounts to 4.1 in the static limit (HF and LC-BLYP) and to 4.7 to 5.1 at λ = 1900 and 1064 nm. These ratios are slightly larger in vacuo. So, although the π-conjugated segments of the collagen chains are small and disjoint, their β_{HRS} responses do not simply evolve linearly with the size of the chain, but rather β_{HRS} is exalted when increasing chain length. This is the result of typical intrachain electrostatic (hyper)polarization effects, which reinforce the electric field parallel to the chain and reduce its components perpendicular to it. Frequency dispersions of β_{HRS} of PPG10 are sketched in Figure 6, exhibiting similar behavior with and without solvent effects as well as at both the HF and LC-BLYP levels of approximation. Note that at λ = 790 nm the difference between HF and LC-BLYP now amounts to ~15%.

Experimentally, for λ = 790 nm, ref 14 reports a value of 11 460 ± 690 au for the β_{HRS} of PPG10 and a DR of 8.7. (It is assumed that ref 14 adopts the T convention.) Although, the wavelength of measurement (790/2 = 395 nm) is quite far from the first one-photon absorption edge (235 nm), the experimental dynamic response was extrapolated to the static limit by adopting different refinements of the TSA (Table 7). The values obtained with the three TSA levels of refinement are consistent and on the order of 7200 au.

Table 7. Measured and Extrapolated Values of β_{HRS} of $[(Pro\text{-}Pro\text{-}Gly)_{10}]_3$ (in au)

$\beta_{HRS,790}$	11460 ± 690
$\beta_{HRS,\infty}$ TSA	7180 ± 440
$\beta_{HRS,\infty}$ TSA (homog. damping)	7100 ± 430
$\beta_{HRS,\infty}$ TSA (homog. + inhomog. damping, vibr.)	7420 ± 450

The experimentally determined DR value of 8.7 is in good agreement with the calculated HF values, from the static DR = 8.8 in vacuo to the dynamic DR = 9.0 at 790 nm. For β_{HRS}, the ONIOM/PCM theoretical values underestimate the experimental results by a factor of two or more, for both static and dynamic quantities. Two remarks should, however, be made because such comparisons are not straightforward. First, water is a dipolar solvent and therefore its static dielectric constant (78.355) is substantially larger than its optical dielectric constant (1.77 for visible light). Because larger dielectric constants lead to an enhancement of β, it is therefore advantageous to compare extrapolated experimental $\beta_{HRS,\infty}$ with β values calculated at optical frequencies far from electronic resonances, where the frequency dispersion is small if not negligible, in our case 1900 nm. Thus, at 1900 nm, β_{HRS} is equal to 3483 au at the HF:HF level and 3521 au at the LC-BLYP:HF level, in comparison with the experimental value of 7420 ± 450 au. This corresponds to an underestimation of 53%, whereas at 790 nm the underestimation reaches 60−63%. This difference (~10%) between the underestimates of the static and dynamic experimental values has to be related to the performance of these methods to predict the excitation energy of the states that dominate the UV/vis absorption spectrum (Figure 3). This first excitation energy amounts to 176 nm at the TDDFT/LC-BLYP level (for one chain of PPG3) in comparison with the experimental 224 nm value, and this overestimation of the excitation energy explains the smaller frequency dispersion.

Second, the experimental value reported in ref 14 was determined by considering water as internal reference for the β_{HRS} measurements, and a value of 65 au from ref 40 was employed for $\beta_{HRS,800}$. Note that other β_{HRS} values for water have been reported in the literature, $\beta_{HRS,800}$ = 58 au[41] and finally $\beta_{HRS,800}$ = 10 au.[42,43] It is therefore difficult to go further in the comparison because the differences between these reference values are quite large, which is a typical difficulty

dx.doi.org/10.1021/jp501602a | J. Phys. Chem. C 2014, 118, 8595−8602

when comparing theoretical/calculated and experimental/measured NLO responses.[44,45]

IV. CONCLUSIONS

First-principles calculations have been performed on the PPG10 compound, a molecular model for the collagen triple-helix structure and its building blocks to unravel the origin and the nature of the first hyperpolarizability of collagen. In agreement with previous investigations, β of the triple helix originates from the amide groups. Their β-tensor components parallel to the helical axis add to each other, whereas the perpendicular components cancel each other, which result in a dipolar first hyperpolarizability and a DR close to 9. The calculations have shown that the resulting β values cannot be viewed as the simple sum of the amide group contributions. Indeed, for a given chain, the β per amino acid increases with the size of the chain, whereas the β of the triple helix is smaller than three times the β of a single chain. These calculations have adopted the ONIOM scheme, of which the reliability for calculating β has been confirmed when combining high and low layers described with different basis sets. Moreover, comparisons between levels of approximation have demonstrated the weak impact of electron correlation on the first hyperpolarizabilities of collagen building blocks, contrary to many traditional compounds for nonlinear optics, either push−pull π-conjugated systems or reference molecules like CCl_4. Comparison with experiment was hampered by the lack of undisputable reference β value for H_2O.

■ ASSOCIATED CONTENT

Supporting Information

Additional data and figures on the collagen moieties geometries, dipole moments, and first hyperpolarizabilities, including the basis set and dispersion effects on the first hyperpolarizabilities and their unit sphere representations. This material is available free of charge via the Internet at http://pubs.acs.org.

■ AUTHOR INFORMATION

Corresponding Author

*E-mail: benoit.champagne@unamur.be. Tel: +32 (0)81 72 45 54.

Notes

The authors declare no competing financial interest.

■ ACKNOWLEDGMENTS

J. de R. thanks the F.R.S.-FNRS for his postdoctoral researcher position. We appreciate help from Mrs. B. Norberg from the Université de Namur for the UV measurements and Dr. Georges Feller from the University of Liège for the DLS characterizations. We also thank Prof. Th. Verbiest and Dr. S. Van Cleuvenbergen for fruitful discussions. The calculations were performed on the computing facilities of the Consortium des Équipements de Calcul Intensif (CÉCI, http://www.ceci-hpc.be), in particular, those of the Plateforme Technologique de Calcul Intensif (PTCI) installed in the University of Namur, for which we gratefully acknowledge financial support of the FNRS-FRFC (Convention No. 2.4.617.07.F and 2.5020.11) and of the University of Namur.

■ REFERENCES

(1) Campagnola, P. J.; Loew, L. M. Second-Harmonic Imaging Microscopy for Visualizing Biomolecular Arrays in Cells, Tissues and Organisms. *Nat. Biotechnol.* **2003**, *21*, 1356−1360.
(2) Reeve, J. E.; Anderson, H. L.; Clays, K. Dyes for Biological Second Harmonic Generation Imaging. *Phys. Chem. Chem. Phys.* **2010**, *12*, 13484−13498.
(3) Abraham, T.; Hirota, J. A.; Wadsworth, S.; Knight, D. A. Minimally Invasive Multiphoton and Harmonic Generation Imaging of Extracellular Matrix Structures in Lung Airway and Related Diseases. *Pulm. Pharmacol. Ther.* **2011**, *24*, 487−496.
(4) Strachan, C. J.; Windbergs, M.; Offerhaus, H. L. Pharmaceutical Applications of Non-Linear Imaging. *Int. J. Pharm.* **2011**, *417*, 163−172.
(5) Huang, S.-H.; Hsiao, C.-D.; Lin, D.-S.; Chow, C.-Y.; Chang, C.-J.; Liau, I. Imaging of Zebrafish *In Vivo* with Second-Harmonic Generation Reveals Shortened Sarcomeres Associated with Myopathy Induced by Statin. *PloS One* **2011**, *6* (e24764), 1−8.
(6) Doras, C.; Taupier, G.; Barsella, A.; Mager, L.; Boeglin, A.; Bulou, H.; Bousquet, P.; Dorkenoo, K. D. Polarization State Studies in Second Harmonic Generation Signals to Trace Atherosclerosis Lesions. *Opt. Express* **2011**, *19*, 15062−15068.
(7) Chen, W.-L.; Hu, P.-S.; Ghazaryan, A.; Chen, S.-J.; Tsai, T.-H.; Dong, C.-Y. Quantitative Analysis of Multiphoton Excitation Autofluorescence and Second Harmonic Generation Imaging for Medical Diagnosis. *Comput. Med. Imaging Graphics* **2012**, *36*, 519−526.
(8) Chen, X.; Nadiarynkh, O.; Plotnikov, S.; Campagnola, P. J. Second Harmonic Generation Microscopy for Quantitative Analysis of Collagen Fibrillar Structure. *Nat. Protoc.* **2012**, *7*, 654−669.
(9) Wu, S.-l.; Li, H.; Zhang, X.-m.; Chen, W.; Wang, Y.-x. Character of Skin On Photo-Thermal Response and its Regeneration Process Using Second-Harmonic Generation Microscopy. *Lasers Med. Sci.* **2014**, *29*, 141−146.
(10) Freund, I.; Deutsch, M.; Sprecher, A. Connective Tissue Polarity. Optical Second-Harmonic Microscopy, Crossed-Beam Summation, and Small-Angle Scattering In Rat-Tail Tendon. *Biophys. J.* **1986**, *50*, 693−712.
(11) Roth, S.; Freund, I. Second Harmonic Generation in Collagen. *J. Chem. Phys.* **1979**, *70*, 1637−1643.
(12) Hulmes, D. J. S. Building Collagen Molecules, Fibrils, and Suprafibrillar Structures. *J. Struct. Biol.* **2002**, *137*, 2−10.
(13) Kadler, K. E.; Baldock, C.; Bella, J.; Boot-Handford, R. P. Collagens at a Glance. *J. Cell Sci.* **2007**, *120*, 1955−1958.
(14) Deniset-Besseau, A.; Duboisset, J.; Benichou, E.; Hache, F.; Brevet, P.-F.; Schanne-Klein, M.-C. Measurement of the Second-Order Hyperpolarizability of the Collagen Triple Helix and Determination of Its Physical Origin. *J. Phys. Chem. B* **2009**, *113*, 13437−13445.
(15) Loison, C.; Simon, D. Additive Model for the Second Harmonic Generation Hyperpolarizability Applied to a Collagen-Mimicking Peptide (Pro-Pro-Gly)10. *J. Phys. Chem. A* **2010**, *114*, 7769−7779.
(16) Tuer, A. E.; Krouglov, S.; Prent, N.; Cisek, R.; Sandkuijl, D.; Yasufuku, K.; Wilson, B. C.; Barzda, V. Nonlinear Optical Properties of Type I Collagen Fibers Studied by Polarization Dependent Second Harmonic Generation Microscopy. *J. Phys. Chem. B* **2011**, *115*, 12759−12769.
(17) Tuer, A.; Krouglov, S.; Cisek, R.; Tokarz, D.; Barzda, V. Three-Dimensional Visualization of the First Hyperpolarizability Tensor. *J. Comput. Chem.* **2011**, *32*, 1128−1134.
(18) Alparone, A. The effect of Secondary Structures on the NLO Properties of Single Chain Oligopeptides: a Comparison Between β-strand and α-helix Polyglycines. *Phys. Chem. Chem. Phys.* **2013**, *15*, 12958−12962.
(19) Wei, J.; Wang, J.-Y.; Zhang, M.-Y.; Chai, G.-L.; Lin, C.-S.; Cheng, W.-D. Single Amino Acid Mutation in Alpha-Helical Peptide Affect Second Harmonic Generation Hyperpolarizability. *Chem. Phys. Lett.* **2013**, *556*, 260−265.
(20) De Meulenaere, E.; Nguyen Bich, N.; de Wergifosse, M.; Van Hecke, K.; Van Meervelt, L.; Vanderleyden, J. Champagne, B.; Clays,

K., Improving the Second-Order Nonlinear Optical Response of Fluorescent Proteins: The Symmetry Argument. *J. Am. Chem. Soc.* **2013**, *135*, 4061−4069.
(21) Dapprich, S.; Komáromi, I.; Byun, K. S.; Morokuma, K.; Frisch, M. J. A New ONIOM Implementation in Gaussian98. Part I. The Calculation of Energies, Gradients, Vibrational Frequencies and Electric Field Derivatives. *J. Mol. Struc.: THEOCHEM* **1999**, *461*−*462*, 1−21.
(22) Berisio, R.; Vitagliano, L.; Mazzarella, L.; Zagari, A. Crystal Structure of the Collagen Triple Helix Model $[(\text{Pro-Pro-Gly})_{10}]_3$. *Protein Sci.* **2002**, *11*, 262−270.
(23) Tomasi, J.; Persico, M. Molecular Interactions in Solution: An Overview of Methods Based on Continuous Distributions of the Solvent. *Chem. Rev.* **1994**, *94*, 2027−2094.
(24) Tomasi, J.; Mennucci, B.; Cammi, R. Quantum Mechanical Continuum Solvation Models. *Chem. Rev.* **2005**, *105*, 2999−3094.
(25) Vreven, T.; Mennucci, B.; da Silva, C. O.; Morokuma, K.; Tomasi, J. The ONIOM-PCM method: Combining the Hybrid Molecular Orbital Method and the Polarizable Continuum Model for Solvation. Application to the Geometry and Properties of a Merocyanine in Solution. *J. Chem. Phys.* **2001**, *115*, 62−72.
(26) de Wergifosse, M. Champagne, B., Electron Correlation Effects on the First Hyperpolarizability of Push-Pull π-conjugated Systems. *J. Chem. Phys.* **2011**, *134* (074113), 1−13.
(27) Yanai, T.; Tew, D. P.; Handy, N. C. A New Hybrid Exchange−Correlation Functional Using the Coulomb-Attenuating Method (CAM-B3LYP). *Chem. Phys. Lett.* **2004**, *393*, 51−57.
(28) Tawada, Y.; Tsuneda, T.; Yanagisawa, S.; Yanai, T.; Hirao, K. A Long-Range-Corrected Time-Dependent Density Functional Theory. *J. Chem. Phys.* **2004**, *120*, 8425−8433.
(29) Cohen, H. D.; Roothaan, C. C. J. Electric Dipole Polarizability of Atoms by the Hartree-Fock Method. I. Theory for Closed-Shell Systems. *J. Chem. Phys.* **1965**, *43*, S34−S39.
(30) Sekino, H.; Bartlett, R. J. Hyperpolarizabilities of Molecules with Frequency Dependence and Electron Correlation. *J. Chem. Phys.* **1991**, *94*, 3665−3669.
(31) Verbiest, T.; Clays, K.; Rodriguez, V. *Second-Order Nonlinear Optical Characterization Techniques*, 1st ed.; CRC Press: Boca Raton, FL, 2009.
(32) Bersohn, R.; Pao, Y.-H.; Frisch, H. L. Double-Quantum Light Scattering by Molecules. *J. Chem. Phys.* **1966**, *45*, 3184−3198.
(33) Frisch, M. J.; Trucks, G. W.; Schlegel, H. B.; Scuseria, G. E.; Robb, M. A.; Cheeseman, J. R., Scalmani, G.; Barone, V.; Mennucci, B.; Petersson, G. A.; et al. *Gaussian 09*, revision A.02; Gaussian, Inc.: Wallingford CT, 2009.
(34) Stewart, J. J. P. *MOPAC2009*; Stewart Computational Chemistry: Colorado Springs, CO, 2008. http://OpenMOPAC.net.
(35) Campo, J.; Wenseleers, W.; Goovaerts, E.; Szablewski, M.; Cross, G. H. Accurate Determination and Modeling of the Dispersion of the First Hyperpolarizability of an Efficient Zwitterionic Nonlinear Optical Chromophore by Tunable Wavelength Hyper-Rayleigh Scattering. *J. Phys. Chem. C* **2007**, *112*, 287−296.
(36) Mançois, F.; Pozzo, J.-L.; Pan, J.; Adamietz, F.; Rodriguez, V.; Ducasse, L.; Castet, F.; Plaquet, A. Champagne, B., Two-Way Molecular Switches with Large Nonlinear Optical Contrast. *Chem.—Eur. J.* **2009**, *15*, 2560−2571.
(37) Oudar, J. L.; Chemla, D. S. Hyperpolarizabilities of the Nitroanilines and their Relations to the Excited State Dipole Moment. *J. Chem. Phys.* **1977**, *66*, 2664−2668.
(38) Castet, F.; Bogdan, E.; Plaquet, A.; Ducasse, L.; Champagne, B.; Rodriguez, V. Reference Molecules for Nonlinear Optics: A Joint Experimental and Theoretical Investigation. *J. Chem. Phys.* **2012**, *136* (024506), 1−15.
(39) Méreau, R.; Castet, F.; Botek, E. Champagne, B. Effect of the Dynamical Disorder on the Second-Order Nonlinear Optical Responses of Helicity-Encoded Polymer Strands. *J. Phys. Chem. A* **2009**, *113*, 6552−6554.
(40) Vance, F. W.; Lemon, B. I.; Hupp, J. T. Enormous Hyper-Rayleigh Scattering from Nanocrystalline Gold Particle Suspensions. *J. Phys. Chem. B* **1998**, *102*, 10091−10093.
(41) Clays, K.; Olbrechts, G.; Munters, T.; Persoons, A.; Kim, O.-K.; Choi, L.-S. Enhancement of the Molecular Hyperpolarizability by a Supramolecular Amylose−Dye Inclusion Complex, Studied by Hyper-Rayleigh Scattering with Fluorescence Suppression. *Chem. Phys. Lett.* **1998**, *293*, 337−342.
(42) Campo, J.; Desmet, F.; Wenseleers, W.; Goovaerts, E. Highly sensitive setup for Tunable Wavelength Hyper-Rayleigh Scattering with Parallel Detection and Calibration Data for Various Solvents. *Opt. Express* **2009**, *17*, 4587−4604.
(43) Duboisset, J.; Matar, G.; Russier-Antoine, I.; Benichou, E.; Bachelier, G.; Jonin, C.; Ficheux, D.; Besson, F.; Brevet, P. F. First Hyperpolarizability of the Natural Aromatic Amino Acids Tryptophan, Tyrosine, and Phenylalanine and the Tripeptide Lysine−Tryptophan−Lysine Determined by Hyper-Rayleigh Scattering. *J. Phys. Chem. B* **2010**, *114*, 13861−13865.
(44) Willetts, A.; Rice, J. E.; Burland, D. M.; Shelton, D. P. Problems in the Comparison of Theoretical and Experimental Hyperpolarizabilities. *J. Chem. Phys.* **1992**, *97*, 7590−7599.
(45) Reis, H. Problems in the Comparison of Theoretical and Experimental Hyperpolarizabilities Revisited. *J. Chem. Phys.* **2006**, *125* (014506), 1−9.